Materials and Methods

Metasurface fabrication

As a first step in the fabrication of the Si metasurface, a layer of 660-nm-thick polycrystalline silicon was deposited onto a fused silica wafer via low pressure chemical vapor deposition (LPCVD). Two 100-nm-thick layers of poly-methyl methacrylate (PMMA), namely PMMA 495 and PMMA 950, were consecutively spin coated on Si for electron beam lithography (EBL). A layer of 20-nm-thick Al was also deposited on top of PMMA bilayer via thermal evaporation prior to the EBL to avoid charging effects. PMMA bilayer was then exposed under a 100 keV electron beam, developed for 90 s in methyl isobutyl ketone (MIBK), and rinsed for 30 s in isopropyl alcohol (IPA). After EBL, a layer of 40 nm-thick Al was deposited onto the sample via electron-beam evaporation for lift-off. Using this layer of Al as an etch mask, inductively-coupled-plasma reactive ion etching (ICP-RIE) were performed to etch the Si layer at 15 °C, forming standing Si nanowires with high aspect ratio. This ICP-RIE recipe uses a gas mixture of SF_6 and C_4F_8, with ICP power of 1200 W and radio frequency (RF) power of 15 W. The fabrication is finalized by sequentially soaking the wafer in post-etch residue remover (80 °C for 30 minutes) and Type-A aluminum etchant (40 °C for 4 minutes) to remove the etch residue and the Al etch mask, respectively.

Polarizer fabrication

A 150-nm-thick Al layer was deposited on the fused silica substrate using electron beam evaporation. Afterwards, a layer of 300-nm-thick PMMA was coated on the Al layer and patterned into 500-μm-long lines with a period of 200 nm and linewidth of 70 nm, arrayed over an area of 500 μm by 4 cm to be readily aligned with the entire metasurface area. The line patterns in the PMMA layer were transferred into the Al layer via ICP-RIE, which was performed with a gas mixture of BCl_3, CH_4, and Cl_2, ICP power of 300 W, and RF power of 100 W. Finally, the PMMA etch mask was removed by solvent.

Phase modulating metasurface design:

The color-map depicting the values of L required to achieve an arbitrary phase $\varphi(\text{mod}, 2\pi)$ at any wavelength λ is calculated at $N = 401$ discrete wavelengths given by $\lambda_k = (k + 800)$ nm, where k is an integer varying from -200 to 200 (shown in Fig. 1B). The phase modulating metasurfaces consisted of Si pillars of square cross-section of side-length L ranging from $0.15p_i$ to $0.85p_i$, where p_i is the pitch of the unit cell. For each discrete wavelength λ_i, p_i is chosen to be $p_i = \lambda_i/1.45$. Using the color map of Fig. 2B, along with the wavelength λ to lateral-location x mapping (given approximately by the linear function $\lambda(x)$ of slope -8.78 nm/mm, the metasurface layout consisting of square pillars of lateral location dependent lengths $L(x)$ can be designed to impose any arbitrary spectral phase $\varphi_{i,j}$.

Simultaneous phase and amplitude modulating metasurfaces design:

Color-maps depicting the values of L_x and L_y respectively, required to achieve an arbitrary phase $\varphi_x(\text{mod}, 2\pi)$ is calculated at 401 discrete wavelengths given by $\lambda_k = (k + 800)$ nm, where k is an integer varying from -200 to 200 (shown in Fig. 3D). The simultaneous amplitude and phase modulating metasurfaces consist of Si pillars of rectangular cross-section (acting as half-wave plates with length L_x and width L_y pairs ranging from $0.15p_i$ to $0.85p_i$, where p_i pitch of the unit cell. For each discrete wavelength λ_i, the corresponding value of p_i is shown in Suppl. Fig. S9. In addition, the transmission amplitude at each discrete wavelength λ_i, is conferred through rotation

angle θ of the nanopillar half-wave plates. Using the same ν to x mapping, the corresponding lateral location dependent size of rotated rectangles $(L_x(x), L_y(x))$ and their rotation $\theta(x)$ determine the final metasurface layout to achieve simultaneous amplitude and phase modulation.

Experimental setup:

In the Fourier transform setup for this study, an optical pulse is first angularly dispersed by a grating into the first diffraction order, and then focused by an off-axis metallic parabolic mirror. The input beam has a diameter of 2 cm. The grating is blazed with 300 grooves/mm. The parabolic mirror has a reflected focal length of 381 mm, with an off-axis angle of 15 °. The grating-parabolic mirror-pair is used to spatially disperse the optical pulse over the full length of one or more cascaded metasurfaces, following a quasi-linear function $\lambda(x)$. The beam size and grating combine to give a grating resolvance $R = 200\ \text{mm} \times 300\ \text{grooves/mm} = 6000$, which corresponds to a wavelength resolution of about 0.13 nm at the center wavelength of 800 nm. Under ray tracing, the astigmatism-limited spot size near focus, along the x-direction, is approximately 0.02 mm, as shown in Suppl. Fig. S1. This spot size corresponds to a wavelength resolution of about 0.16 nm after considering the function $\lambda(x)$ as shown in Fig. S2. Along the y-direction, the largest astigmatism-limited spot at the edge of the spectrum is approximately 0.2 mm. The effective numerical aperture of the parabolic mirror is NA = 0.026, which leads to a diffraction-limited spot size of $0.61\lambda/\text{NA} = 0.018$ mm at the center wavelength of λ = 800 nm. We conservatively estimate that the accumulation of these non-idealities leads to an effective monochromatic spot size of approximately 0.037 mm, which corresponds to a wavelength resolution of about 0.33 nm or a frequency resolution of 150 GHz.

Metasurface devices are inserted within the focal volume about the Fourier plane to help achieve the required net masking function. After passing through the metasurfaces, the beam is recombined using a second parabolic mirror and grating pair, yielding a shape-modified pulse of desired temporal characteristics. The metasurfaces are illuminated using a Ti:Sapphire oscillator generating $\lesssim$10 fs pulses, centered at 800 nm (FWHM bandwidth of ≈ 60 THz), with a repetition rate of 75 MHz. The characteristics of the recombined pulse exiting the system, *i.e.* spectral amplitude and phase, are measured using the SPIDER technique (*34*).

Supplementary Text

Jones Matrix for independent amplitude & phase modulation:

We assume that an input light polarized along the with *x*-axis first passes through an optical element described by a Jones matrix J_S and then a linear polarizer aligned to transmit *x*-polarized light. The final polarization state of the output light can be given by:

$$\begin{pmatrix} te^{j\varphi} \\ 0 \end{pmatrix} = \begin{pmatrix} 1 & 0 \\ 0 & 0 \end{pmatrix} J_S \begin{pmatrix} 1 \\ 0 \end{pmatrix} = \begin{pmatrix} 1 & 0 \\ 0 & 0 \end{pmatrix} \begin{pmatrix} J_{11} & J_{12} \\ J_{21} & J_{22} \end{pmatrix} \begin{pmatrix} 1 \\ 0 \end{pmatrix}, \tag{S1}$$

where $te^{j\varphi}$ is the complex amplitude of the masking function a specific frequency component. Multiplying out the matrices gives:

$$\begin{pmatrix} te^{j\varphi} \\ 0 \end{pmatrix} = \begin{pmatrix} J_{11} \\ 0 \end{pmatrix}. \tag{S2}$$

Now consider a birefringent metasurface element with the fast(slow) axis aligned along the x(y) direction. It can be described by a diagonal Jones matrix:

$$\boldsymbol{M_0} = \begin{pmatrix} \mathrm{M}_{11} & 0 \\ 0 & \mathrm{M}_{22} \end{pmatrix} = \begin{pmatrix} e^{j\varphi_x} & 0 \\ 0 & e^{j\varphi_y} \end{pmatrix}, \tag{S3}$$

where M_{11} and M_{22} are the complex transmission coefficients for the x- and y-polarized light. Now if the birefringent element is rotated counter-clockwise by an angle θ, the resulting Jones matrix is then given by:

$$\boldsymbol{M}(\theta) = \boldsymbol{R}(-\theta)\boldsymbol{M_0}\boldsymbol{R}(\theta) = \begin{pmatrix} \cos\theta & -\sin\theta \\ \sin\theta & \cos\theta \end{pmatrix} \begin{pmatrix} e^{j\varphi_x} & 0 \\ 0 & e^{j\varphi_y} \end{pmatrix} \begin{pmatrix} \cos\theta & \sin\theta \\ -\sin\theta & \cos\theta \end{pmatrix}, \tag{S4}$$

where $\boldsymbol{R}(\theta)$ is the rotation matrix. Inserting (S4) into (S1) then yields:

$$te^{j\varphi} = J_{11} = e^{j\varphi_x}\cos^2\theta + e^{j\varphi_y}\sin^2\theta. \tag{S5}$$

Finally, consider the special case when the birefringent metasurface element represents a half-wave plate by enforcing:

$$\frac{e^{j\varphi_x}}{e^{j\varphi_y}} = e^{\pm j\pi} = -1. \tag{S6}$$

Inserting (S6) into (S5) yields:

$$te^{j\varphi} = e^{j\varphi_x}(\cos^2\theta - \sin^2\theta) = \cos(2\theta)e^{j\varphi_x}. \tag{S7}$$

Note that for the designed metasurface/polarizer combination, the amplitude of the transmission coefficient is solely determined by rotation angle θ via $t = \cos(2\theta)$ and the phase of that is determined by the pillar length L_x and width L_y through the color map of Fig. 3D.

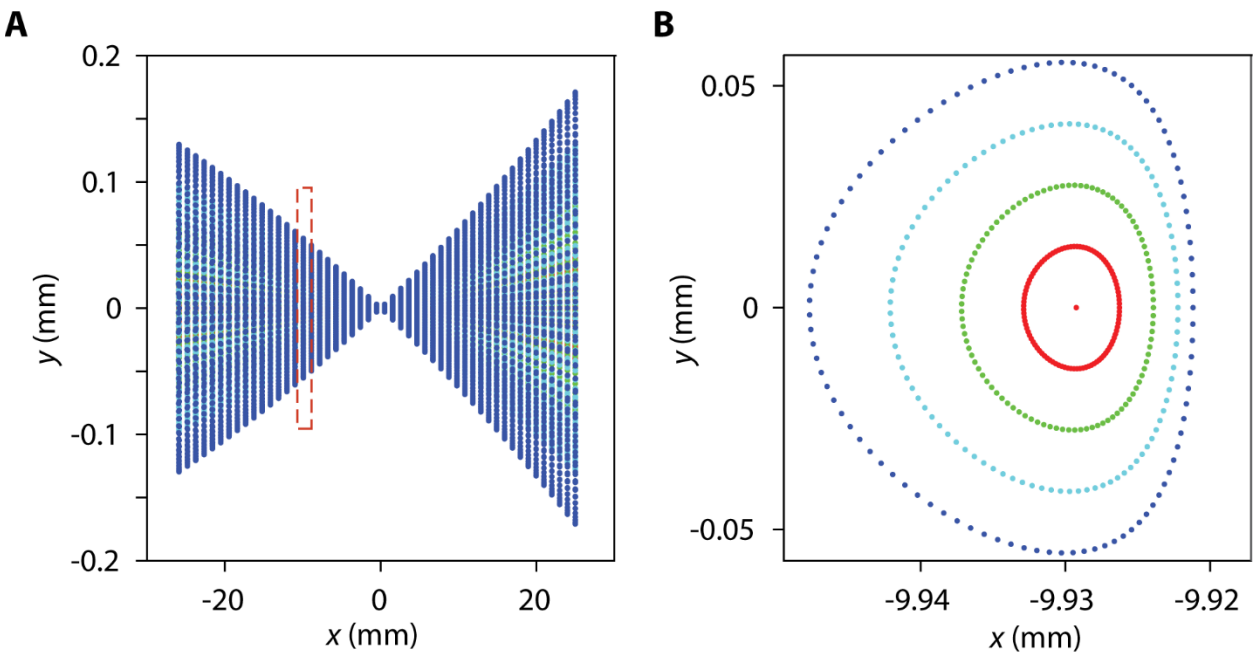

Fig. S1. Ray tracing spot diagrams of the optical setup. The frequency component at 800 nm is assumed to strike the mirror along the optical axis. (**A**) A spot diagram showing astigmatism-limited spots near focus for light of wavelengths between 580 nm (right-most spots, near x = 25 mm) and 1024 nm (left-most spots, near $x = -25$ mm). These individual spot diagrams, for various wavelengths, appear as vertical lines because of the greatly different scaling of the x and y axes. (**B**) A representative zoomed-in spot diagram for an incident beam of radius 1 cm at a wavelength of 886 nm (a zoomed version of the dashed red box in (**A**) near $x = -10$ mm). The red, green, light blue, and dark blue spots represent rays at a position of 0.25, 0.5, 0.75, and 1.0 times the radius of the incident beam, respectively.

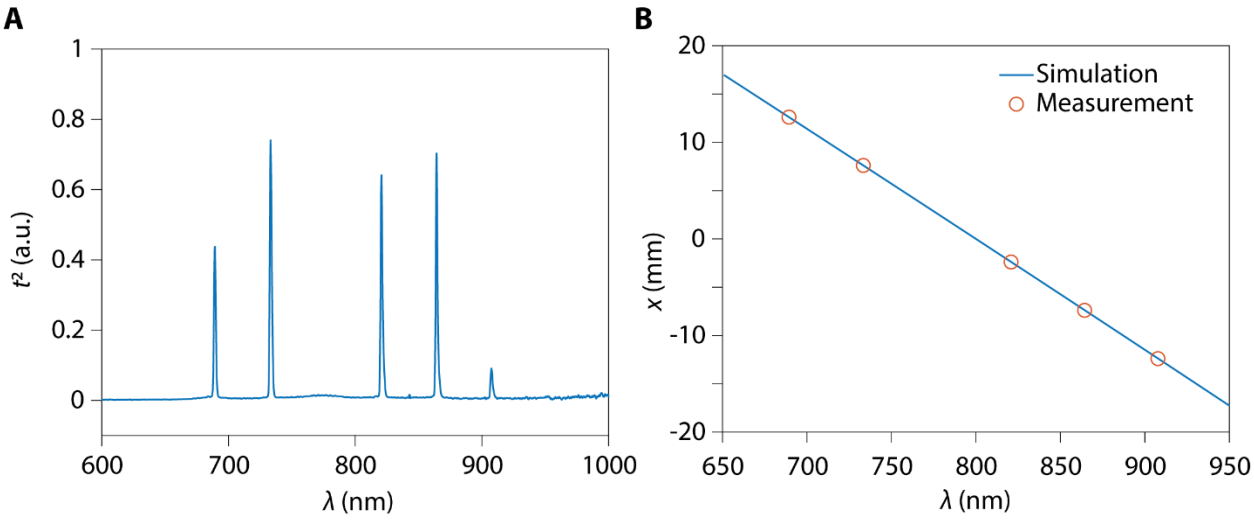

Fig. S2. Quasi-linear mapping of $\lambda(x)$. (**A**) Representative spectrum of the pulse transmitted through a reference modulation mask consisting of two sets of pinholes, each having two or three holes, respectively. The numbers of holes in each group are asymmetric for the ease of calibration. The hole pitch for each group is 5 mm. The reference modulation mask was translated along the x-axis at multiple locations to confirm the mapping of $\lambda(x)$. (**B**) The calibrated relation between x-position and wavelength λ at the Fourier plane. The red circles correspond to the peaks in (**A**) and the blue line corresponds to the simulated $\lambda(x)$ of the optical system using ray tracing. $\lambda(x)$ can be fitted with a linear function $\lambda(x) = -8.78\ \mathrm{nm/mm} \cdot x + 800\ \mathrm{nm}$.

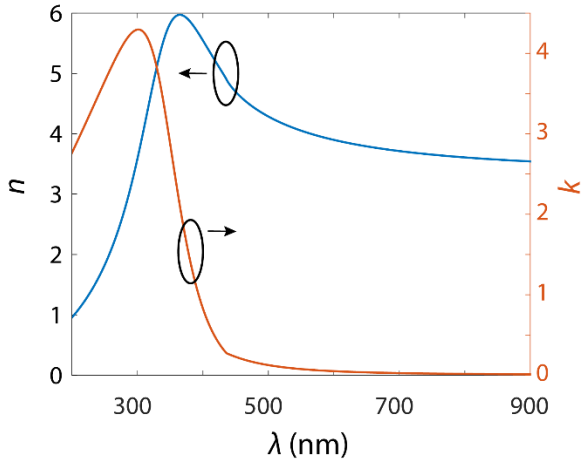

Fig. S3. Refractive index of polycrystalline silicon. The real (n) and imaginary part (k) of the refractive index of LPCVD Si, deposited on an oxide coated reference Si substrate (thermal oxide thickness = 300 nm), and measured using spectroscopic ellipsometry. The values for both n and k are within 2 % corresponding to one standard deviation in the ellipsometry measurement.

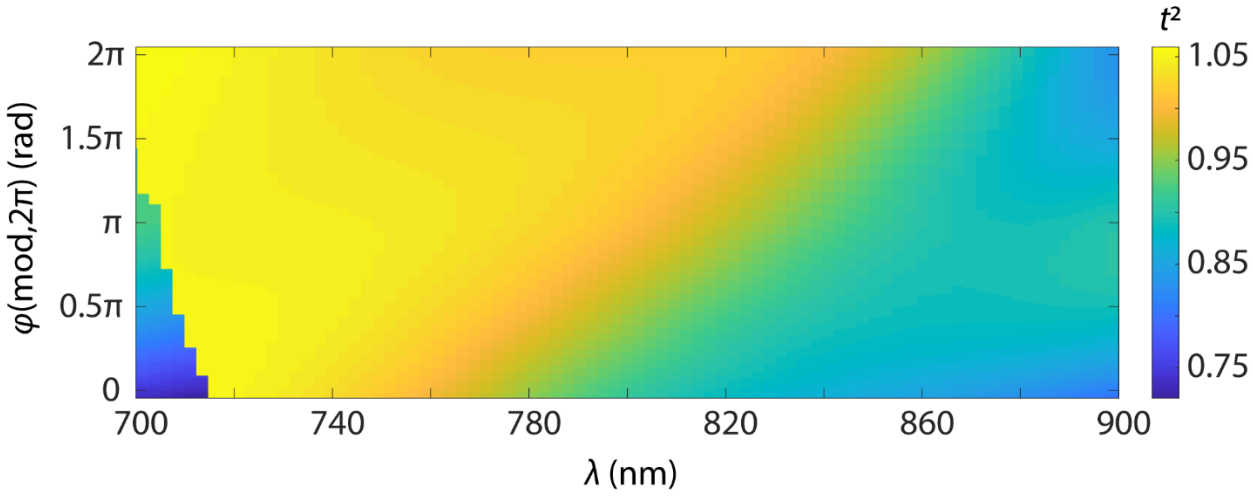

Fig. S4. Color-map of the calculated amplitude transmission coefficient t^2. Calculated t^2 corresponding to the phase-manipulating metasurfaces discussed in Fig. 2. The transmission amplitude remains > 70 % for any choice of L (required to achieve an arbitrary phase φ(mod, 2π) at any wavelength λ) in the phase manipulating metasurface.

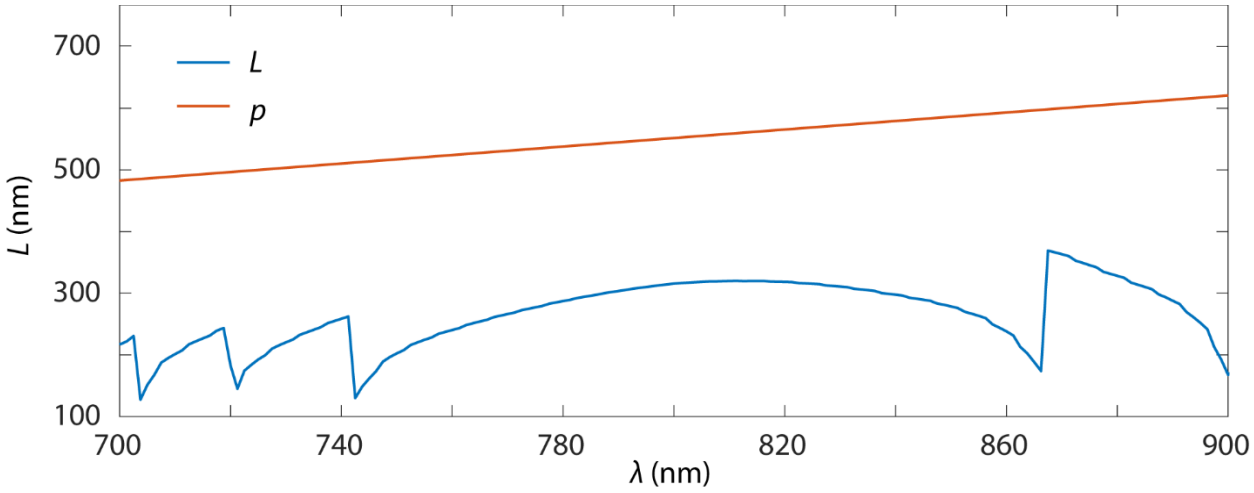

Fig. S5. Side-length *L* of the nanopillar and lattice constant *p* vs. the wavelength *λ*. Retrieved using the procedure described in Methods to achieve the quadratic spectral phase plotted in Fig. 2C.

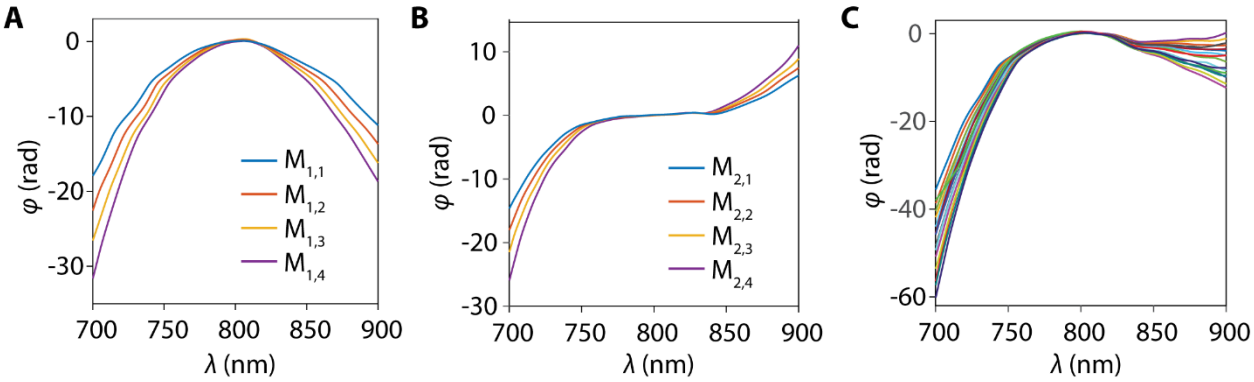

Fig. S6. Targeted designs for cascading phase manipulating metasurfaces. (**A**) Targetd (**B**) Targetd Four quadratic masking functions $m_{1,j}(x) = e^{i\varphi_{1,j}(\nu(x))}$ (j = 1, 2, 3, and 4) implemented on S_1, where $\varphi_{1,j}(\nu) = -A_{1,j}(\nu - \nu_0)^2$, $A_{1,1} = 6 \times 10^{-3}$ rad/THz^2, $A_{1,2} = 7 \times 10^{-3}$ rad/THz^2, $A_{1,3} = 8 \times 10^{-3}$ rad/THz^2, and $A_{1,4} = 9 \times 10^{-3}$ rad/THz^2. (**B**) Four cubic masking functions $m_{2,j}(x) = e^{i\varphi_{2,j}(\nu(x))}$ (j = 1, 2, 3, and 4) implemented on S_2, where $\varphi_{2,j}(\nu) = -A_{2,j}(\nu - \nu_0)^3$, $A_{2,1} = 7 \times 10^{-5}$ rad/THz^3, $A_{2,2} = 9 \times 10^{-5}$ rad/THz^3, $A_{2,3} = 1.1 \times 10^{-4}$ rad/THz^3, and $A_{2,4} = 1.3 \times 10^{-4}$ rad/THz^3. (C) 16 spectral phase shift masking functions available through cascading S_1 and S_2.

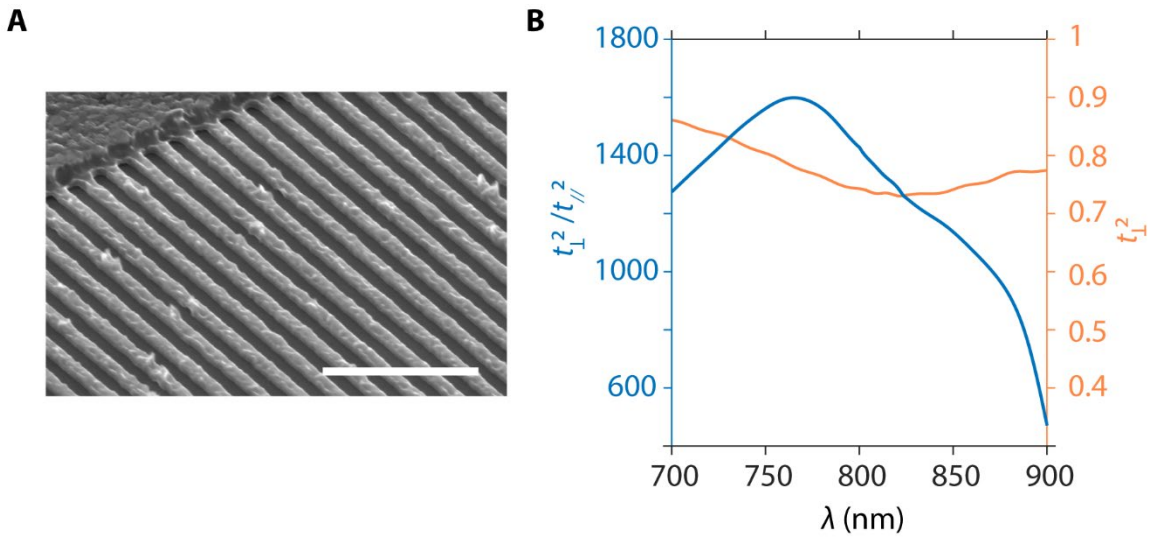

Fig. S7. Experimental characterization of the thin-film wire-grid polarizer designed for the simultaneous phase and amplitude manipulating metasurface discussed in Fig. 3. (**A**) A representative SEM image (52 ° perspective view) of the wire polarizer fabricated for this study. The polarizer wires consist of 200 nm-wide and 500 μm-long Al nanowires, positioned in a one-dimensional lattice with pitch of 200 nm along the *x*-direction. Scale bar represents 1 μm. (**B**) Experimentally measured extinction ratio ($t_\perp^2/t_{//}^2$) and relative power transmittance $t_\perp^2$ *vs.* the wavelength λ of the wire polarizer, where $t_\perp^2$ is the power transmittance for the input-polarization orthogonal to the wires and $t_{//}^2$ is that for the polarization parallel to the wires.

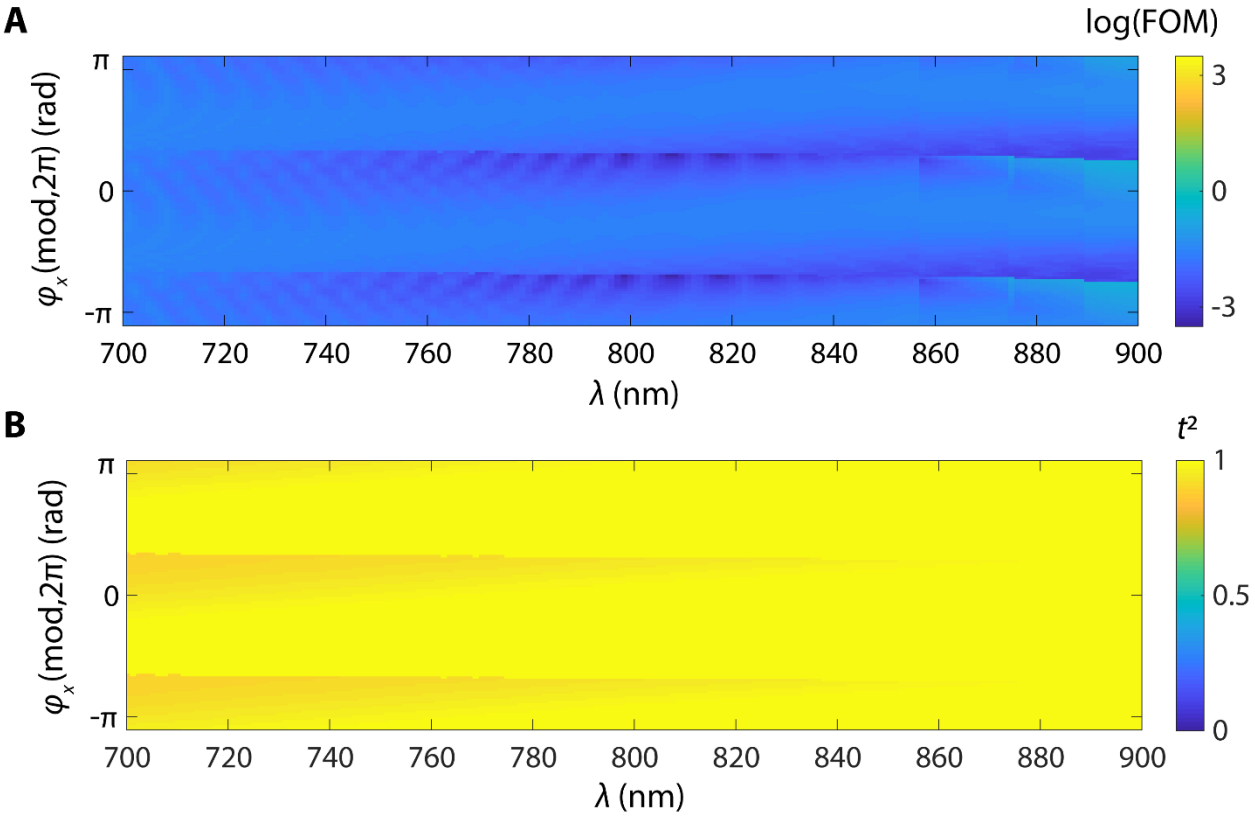

Fig. S8. Color-map of the calculated *FOM* and transmission coefficient t_x^2 for the phase & amplitude modulation mask design. (A, B) Color-maps depicting the *FOM* and relative transmission intensity t^2 respectively, *vs.* the wavelength $\boldsymbol{\lambda}$ for any arbitrary phase φ_x(mod, 2π) at any wavelength, calculated for corresponding L_x and L_y pair values used in Fig. 3D.

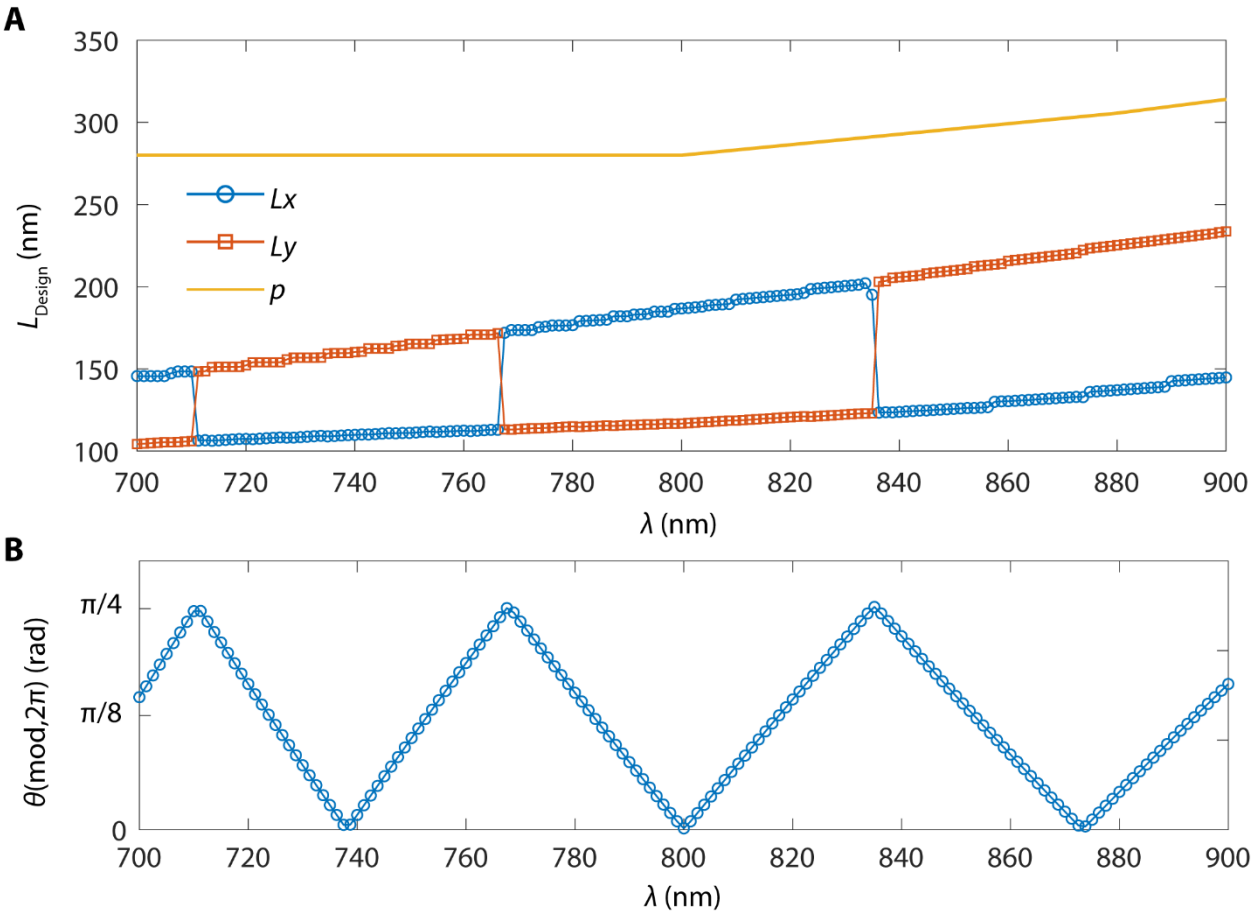

Fig. S9. Layout design parameters for the pulse splitting metasurface. (**A**) Rectangular nanopillar length L_x and width L_y for each wavelength λ_k along with k-th corresponding pitch p_k used to implement the required phase function in Fig. 3E. The pitch p was optimized for 2π coverage at five wavelengths 700 nm, 750 nm, 800 nm, 840 nm, and 900 nm within the pulse bandwidth, and p_k at each λ_k was determined through interpolation. L_x, L_y pairs are determined using the procedure described in the Methods section. (**B**) Rotation angle of the nanopillars θ_k for each wavelength λ_k to implement the targeted amplitude function of Fig. 3F.